Cooperative Jahn-Teller Phase Transition in $LaMnO_3$ Studied by X-Ray Absorption Spectroscopy

M. C. Sánchez,[1] G. Subías,[1,2] J. García,[1,*] and J. Blasco[1]

[1]*Instituto de Ciencia de Materiales de Aragón, Consejo Superior de Investigaciones Científicas y Universidad de Zaragoza, 50009 Zaragoza, Spain*

[2]*European Synchrotron Radiation Facility, Boite Postale 220, 38043 Grenoble, France*

(Received 2 October 2002; published 31 January 2003)

The local structure of $LaMnO_3$ across the Jahn-Teller (JT) transition at $T_{JT} = 750$ K was studied by means of x-ray absorption near edge structure and extended x-ray absorption fine structure at the Mn K-edge. Our results indicate a similar electronic local structure for Mn atoms above and below T_{JT} and a dynamical tetragonal JT distortion of MnO_6 octahedra above T_{JT}. The structural transition is originated by the ordering of tetragonally distorted octahedra. The entropy content of the transition is analyzed within the framework of the three-state Potts model with nearest neighbor antiferrodistortive coupling.

DOI: 10.1103/PhysRevLett.90.045503 PACS numbers: 61.10.Dp, 61.10.Eq, 71.90.+q

$LaMnO_3$ is the mother material of colossal magnetoresistance manganites [1,2]. At ambient conditions stoichiometric $LaMnO_3$ is a paramagnetic insulator with orthorhombic perovskite structure (space group Pbnm [3,4]). In this structure, alternating long and short Mn-O bonds lie in the ab plane along the Mn-O-Mn path. This kind of arrangement is the signature of orbital ordering (OO) which is established owing to the cooperative Jahn-Teller effect. The tetragonal distortion breaks the degeneracy of the e_g orbital in the $t_{2g}^3 e_g^1$ electronic configuration of the Mn^{3+} ions and stabilizes the $3d_{z2\text{-}r2}$ orbital with respect to the $3d_{x2-y2}$ ones. A-type antiferromagnetism below $T_N = 140$ K was explained as arising from this orbital ordering [5,6]. $LaMnO_3$ undergoes a structural phase transition at $T_{JT} = 750$ K above which the orbital ordering disappears [4,7]. This transition is accompanied by an abrupt change in the electrical resistivity, thermoelectric power, and Weiss constant [8].

Several mechanisms have been proposed to explain the orbital ordering in $3d$ transition metal oxides with orbital degeneracy. Some authors attribute it to the superexchange interaction between atoms in different sites [9,10]. Other authors claim that the lattice distortion occurs cooperatively at T_{JT} and simultaneously lifts the orbital degeneracy [11–13]. Other mechanisms, including the combined influence of superexchange and electron-phonon interactions, have also been proposed [14,15]. High resolution neutron diffraction experiments show nearly regular MnO_6 octahedra at $T > T_{JT}$ without change of crystal symmetry though thermal parameters for oxygen atoms are unusually high [4]. A pseudocubic lattice would arise from the average of dynamic spatial fluctuations of the orthorhombic distortion. In this framework, Zou and Goodenough [8] proposed a vibronic mechanism to explain the electrical conductivity above T_{JT}.

In spite of the theoretical effort to understand orbital ordering in $LaMnO_3$ [9–16], direct experimental evidences shedding light on the mechanism responsible for the structural transition at T_{JT} are still missing. X-ray absorption spectroscopy gives direct information on the electronic and geometrical structure around the absorbing atom. Moreover, the extremely short interaction time of the x-ray absorption process (10^{-14} s), lower than the one corresponding to the thermal motion, allows us to determine if the MnO_6 octahedron is dynamically distorted above T_{JT}. X-ray absorption near edge structure (XANES) spectra also give us information about the possible electronic changes at the Mn atom at the structural phase transition. Moreover, we have also performed heat capacity experiments to determine the entropy content of the phase transition. These results will demonstrate that MnO_6 octahedra are locally distorted above T_{JT}. The structural phase transition can reasonably be described as an ordering of local distortions that are thermally disordered above T_{JT}.

The preparation and characterization of stoichiometric $LaMnO_3$ was reported elsewhere [3]. X-ray absorption experiments (20 K $\leq T \leq$ 920 K) were performed at the ESRF beam line BM29 (Grenoble, France). A fixed-exit Si(311) double-crystal monochromator was used, the estimated energy resolution being $\Delta E/E = 7 \times 10^{-5}$. Spectra were obtained in transmission mode using ionization chambers as detectors using the experimental setup of the beam line [17]. XANES spectra were normalized to the high part of the spectrum (100 eV) after a linear background subtraction [18]. Extended x-ray absorption fine structure (EXAFS) spectra [$\chi(k)$] were obtained by removing the smooth atomic absorption coefficient (μ_0) by means of a cubic spline [18]. The spectra were analyzed using the FEFF 8.10 code that allows correlating the Debye-Waller factor (DW) with

the interatomic distances. The structural analysis was performed in the R-space fitting mode including multiple scattering terms up to 4 Å [19]. Heat capacity was measured in a Perkin-Elmer DSC apparatus after calibration with indium.

XANES spectra for several temperatures below and above T_{JT} are shown in Fig. 1. The spectral shape for $LaMnO_3$ is the same as previously published [20–23]. It is composed by the preedge region, where transitions to empty Mn d states are brought by the covalency with the adjacent oxygen p states, and the main-edge region corresponding to dipolar transitions to the empty Mn p-band. The spectra at different temperatures are alike, indicating that no large changes of the local electronic structure occur between 300 and 920 K. The spectra shift to lower energies with increasing temperature, the maximum shift being of about 0.5 eV. The same features are observed in the preedge energy region, indicating the same splitting of Mn d orbitals below and above T_{JT}. The fact that these differences are small can be attributed to an increase of atomic vibrations that smooth out the absorption features. Accordingly, the absorption edge shifts apparently and the main peak becomes broader. To check the presence of small changes at temperatures close to T_{JT}, the spectra obtained at successive temperatures were subtracted from each other. The difference is plotted in the inset of Fig. 1. The largest difference corresponds to the 650 K–750 K temperature range, close to T_{JT}, giving direct signature of the phase transition.

EXAFS spectra of $LaMnO_3$ were obtained at fixed temperatures from 20 K up to 920 K. The spectra at low temperatures ($T < 300$ K) were measured up to $k = 12$ Å^{-1} in order to obtain reliable structural parameters. For instance, Fig. 2 shows the EXAFS spectrum at 20 K,

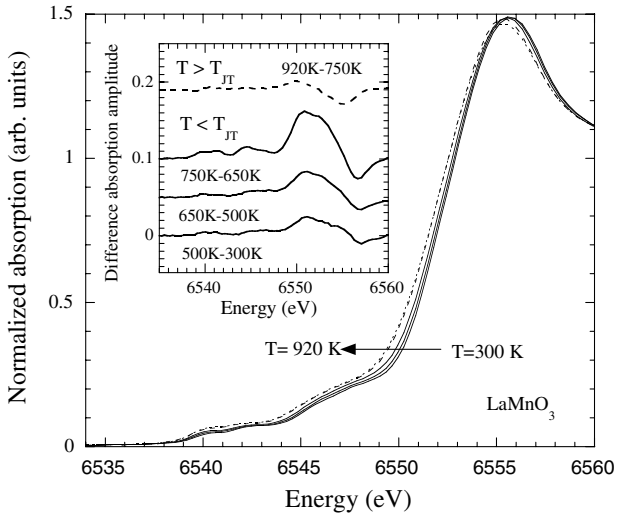

FIG. 1. Normalized XANES spectra of $LaMnO_3$ as a function of temperature. A small shift of the spectra is shown increasing temperature. The inset shows the difference between spectra taken at successive temperatures. The largest difference is observed at T_{JT}.

its Fourier transform (FT), and the best-fit result. The obtained interatomic distances are in good agreement with those obtained by diffraction techniques [4]. The FT of the spectra above room temperature is shown in Fig. 3. We observe that the intensity of the different peaks, associated to different coordination shells, decreases with increasing temperature. It is noteworthy that there is no discontinuity in the EXAFS spectra crossing T_{JT}, indicating a similar local structure for the Mn^{3+} ions above and below T_{JT}. If the tetragonal distortion would disappear at the phase transition, the intensity of the first oxygen shell peak would increase above T_{JT}, owing to a more symmetrical oxygen environment. In order to verify it, the Fourier filtered spectra between 1 and 2 Å (first oxygen coordination shell) at different temperatures were fitted with the corresponding at room temperature. These spectra can be well reproduced from the room-temperature spectrum by changing only the relative DW ($\Delta\sigma$) factor. The obtained $\Delta\sigma$ increases with increasing temperature as expected for a system with no variation in the local structure. In order to quantify the tetragonal distortion,

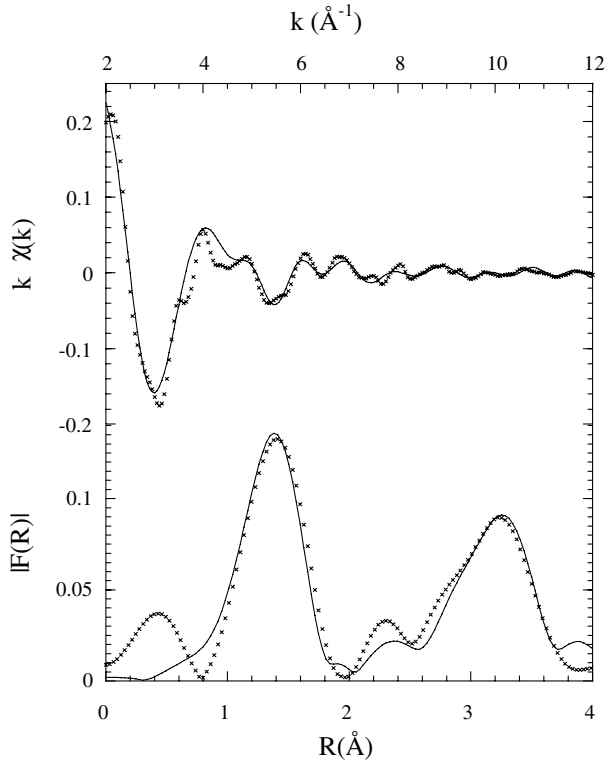

FIG. 2. Upper figure: EXAFS spectra of $LaMnO_3$ (dotted line) measured at 20 K compared with the best fit (solid line), first and second shells were considered. Lower figure: Fourier transform of this spectra. The relevant structural parameters of the fit for the 20 K spectrum are the following: Mn-O, $N_1 = 4$, $d_1 = 1.92$ Å, $\sigma_1^2 = 0.0016$ Å^2; $N_2 = 2$, $d_2 = 2.13$ Å, $\sigma_2^2 = 0.0018$ Å^2; Mn-La, $N = 2$, $d_1 = 3.22$ Å, $d_2 = 3.33$ Å, $d_3 = 3.42$ Å, and $d_4 = 3.71$ Å, $\sigma^2 = 0.0007$ Å^2; Mn-Mn, $N_1 = 2$, $d_1 = 3.79$ Å, $N_2 = 4$, $d_2 = 3.95$ Å, $\sigma^2 = 0.001$ Å^2.

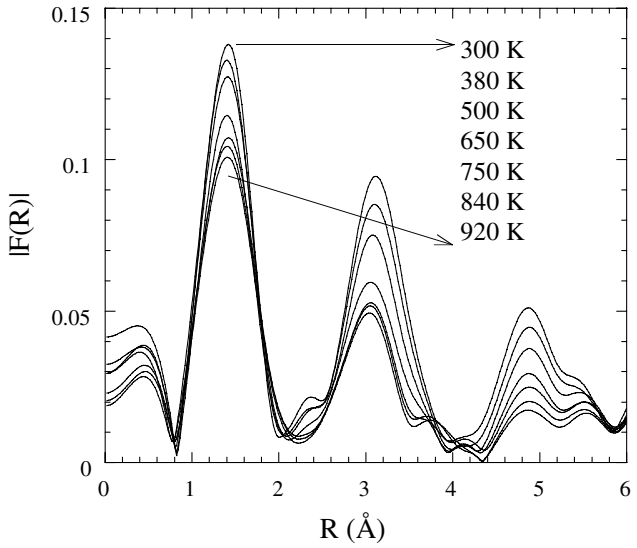

FIG. 3. Fourier transform of the EXAFS spectra of $LaMnO_3$ taken at fixed temperatures between room temperature and 920 K. The different peaks corresponding to different coordination shells decrease as the temperature increases.

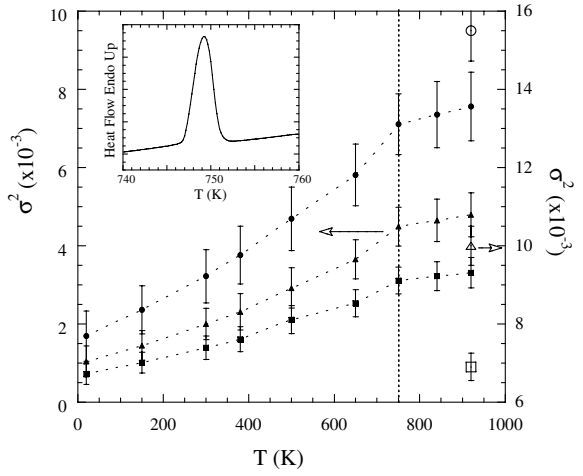

FIG. 4. Debye-Waller factor as a function of temperature for the three coordination shells (circles Mn-O, triangles Mn-Mn, and squares Mn-La). The vertical line indicates T_{JT}. DW factors obtained from a unique Mn-O distance at 920 K are also shown (open symbol and scale on the right). The inset shows heat capacity anomaly at the JT phase transition.

we have used the FEFF 8.10 code to fit the spectra. First and second coordination shells were included in the fitting process and multiple scattering paths were also considered. The obtained interatomic Mn-X (X = O, Mn, La) distances agree with the crystallographic values, except for $T > T_{JT}$. Our results show that the local structure does not change appreciably at the phase transition. For instance, the interatomic distances obtained from the fit at 840 K are $d(\text{Mn-O}_{\text{short}}) = 1.92$ Å, $d(\text{Mn-O}_{\text{long}}) = 2.13$ Å, $d(\text{Mn-Mn}_{\text{short}}) = 3.85$ Å, and $d(\text{Mn-Mn}_{\text{long}}) = 4.01$ Å, close to the room-temperature values. Figure 4 shows DW factors of the different Mn-X contributions as a function of temperature. A small change in the $\sigma^2(T)$ variation is observed at the phase transition for the Mn-O, Mn-La, and Mn-Mn shells. Moreover, the comparison of Mn-O and Mn-Mn DW factors indicates a strong correlation between the fluctuations of adjacent Mn-O bonds. Finally, we tried to fit the high temperature spectra using the reported high temperature structure in Ref. [4]. The fits are markedly worse in this case and the obtained DW parameters are unusually high (comparable to the tetragonal JT distortion) as shown in Fig. 4.

In conclusion, EXAFS spectra show that the MnO_6 octahedra are also tetragonally distorted for $T > T_{JT}$. The interaction time for the photoabsorption process is smaller than for that corresponding to the thermal motion. Consequently, EXAFS probe the instantaneous local structure around the absorbing atom. On the other hand, diffraction data provide the periodicity of the average structure as Rodriguez-Carvajal *et al.* [4] claim. From both experiments, we can infer that below T_{JT} the tetragonal local distortion is ordered in space giving rise to the well-known Pbnm structure. However, above T_{JT}, the local distortions are dynamically disordered and the average lattice is cubic. This result shows that Mn^{3+} ions exhibit a strong Jahn-Teller coupling which leads to the called static JT regime [24]. In this regime, the potential surface in the Q_3Q_2 plane (Q_3 and Q_2 are normal coordinates of Γ_3 symmetry modes) changes from the well-known Mexican hat to the tricorn with three energy wells. Each Mn octahedron is dynamically distorted at $T > T_{JT}$ changing among the three equivalent tetragonal configurations. Below T_{JT}, the tetragonal distortions are periodically ordered. Thus, the phase transition at T_{JT}, can be classified as an order-disorder phase transition where the statistical occupation in the disordered phase corresponds to the three possible orientations of the tetragonal distortions on each octahedron. The three-state Potts model would be then the appropriate statistical model [25].

Heat capacity measurements of $LaMnO_3$ show a strong anomaly at 750 K (see inset of Fig. 4). A thermal hysteresis of 9 K between the heating and the cooling runs points to the first order character of this transition. The enthalpy and entropy contents for this transition are $\Delta H = 3180 \pm 100\ \text{J mol}^{-1}$ and $\Delta S = (0.515 \pm 0.02)R$ ($R = 8.4144\ \text{J K}^{-1}\,\text{mol}^{-1}$). A model of independent distorted MnO_6 octahedra with three equivalent tetragonal distortions would give $\Delta S = R\ln 3 = 1.098R$, far away from the experimental result. In the $LaMnO_3$ system, the MnO_6 octahedra are not independent as they share oxygen atoms with their nearest neighbors. This introduces a constraint in the degrees of freedom for each octahedron. First of all, we can consider a simplified model with a static Mn sublattice. In this case, if a Mn_1-O distance expands, the oxygen shared O-Mn_2 distance should contract and vice versa. This is equivalent to a three-state Potts model with very strong nearest neighbor antiferrodistortive coupling. However, it is well known that a cubic

three-state Potts model does not order when only nearest neighbor antiferrodistortive coupling exits. The estimated ground state entropy is then $S_g = 0.3673R$ [26], lower than the experimental value. The value of the experimental entropy is between those of the independent octahedra model and the strong antiferrodistortive model. Consequently, nearest neighbor ferrodistortive configurations must also be accessible at $T > T_{JT}$ and a large correlation exists among antiferrodistortive distortions above T_{JT}. The correlation length for the antiferrodistortive coupling in the high temperature phase can be inferred from the configurational entropy for a cubic cluster of MnO_6 octahedra of dimension L. This entropy is given by $S_g(L) = S_g + L^{-3}\ln 6$, where S_g is the entropy of an infinite cube [25]. We obtain, with $\Delta S = Sg(L)$, a value of 2.3 for the correlation length of the antiferrodistortive coupling in the high temperature phase. This implies that both local structures (up to distances a little bit larger than the Mn-Mn distance), the instantaneous one for the high temperature phase and the static one for the low temperature phase, should be alike. This result agrees with the EXAFS experiment, which shows that the local structure (including second shell contribution, $L = 2$) nearly unaltered through the transition. There is also not contradiction with diffraction data because this technique provides the average long range periodic structure. Finally, we propose that the ordering be mediated by the interaction of the local distortions with the elastic strain as judged from the observed change of the crystallographic structure through the transition.

In summary, the following relevant results can be concluded from the performed experiments. (i) The orbital degeneracy of the Mn^{3+} ion is already removed at $T > T_{JT}$. XANES spectroscopy shows that the empty Mn^{3+} electronic d states are unaltered through the JT transition, whereas EXAFS spectroscopy shows that the JT tetragonal distortion remains in the pseudocubic phase. (ii) The structural phase transition is produced by the ordering of the local distortions, which are coupled to the macroscopic strain field. (iii) The lowest energy for the e_g electron correspond to the three possible distortions giving rise to three degenerate vibronic states [24], $d_{x2\text{-}r2}$, $d_{y2\text{-}r2}$, and $d_{z2\text{-}r2}$ being the electronic orbitals of the vibronic state. The electron thermally excited jumps between these states above T_{JT} and is localized in an ordered state below T_{JT}. The orbital ordering proposed for $LaMnO_3$ is then arising from the ordering of local JT distortions. A direct electronic origin for orbital ordering (i.e., superexchange between orbitals, or cooperative Jahn-Teller mechanisms with simultaneous local distortion) lifting the orbital degeneracy, should be discarded. (iv) The high temperature phase can be described as a dynamical locally distorted phase with strong antiferrodistortive first neighbor coupling. A schematic picture of the vibronic conductivity mechanism proposed by Zhou and Goodenough [8] could be as follows: Above T_{JT}, the e_g electron jumps between the degenerate three orbitals on each Mn^{3+} ion. This electron can also jump to the orbital of the nearest neighbor manganese owing to the covalent Mn-O bond giving rise to the conduction. Although this conduction mechanism is assisted by phonons, it cannot be considered as polaronic. The e_g electrons are ordered and localized at $T < T_{JT}$, and they cannot jump between adjacent octahedra.

This work was supported by the Spanish CICyT Project No. MAT99-0847. The authors thank ESRF for beam time granting.

*Author to whom correspondence should be addressed. Electronic address: jgr@posta.unizar.es

[1] E. Dagotto, J. Hotta, and A. Moreo, Phys. Rep. **344**, 1 (2001).
[2] M. B. Salamon and M. Jaime, Rev. Mod. Phys. **73**, 583 (2001).
[3] C. Ritter *et al.*, Phys. Rev. B **56**, 8902 (1997).
[4] J. Rodríguez-Carvajal *et al.*, Phys. Rev. B **57**, R3189 (1998).
[5] E. O. Wollan and W. C. Koehler, Phys. Rev. **100**, 545 (1955).
[6] J. B. Goodenough, *Magnetism and Chemical Bond* (Interscience, New York, 1963).
[7] P. Norby *et al.*, J. Solid State Chem. **119**, 191 (1995).
[8] J. S. Zhou and J. B. Goodenough, Phys. Rev. B **60**, R15002 (1999).
[9] S. Okamoto, S. Ishihara, and S. Maekawa, Phys. Rev. B **65**, 144403 (2002).
[10] K. I. Kugel and D. I. Khomskii, Zh. Eksp. Teor. Fiz. **64**, 1429 (1973) [Sov. Phys. JETP **37**, 725 (1973)].
[11] G. Schröder and H. Thomas, Z. Phys. B **25**, 369 (1976).
[12] K.-H. Höck, G. Schröder, and H. Thomas, Z. Phys. B **30**, 403 (1978).
[13] A. J. Millis, Phys. Rev. B **53**, 8434 (1996).
[14] N. Nagaosa, S. Murakami, and H. C. Lee, Phys. Rev. B **57**, R6767 (1998).
[15] J. Bala, A. M. Olés, and G. A. Sawatzky, Phys. Rev. B **65**, 184414 (2002).
[16] P. Ravindran *et al.*, Phys. Rev. B **65**, 064445 (2002), and references therein.
[17] A. Filipponi *et al.*, Rev. Sci. Instrum. **71**, 2422 (2000).
[18] D. C. Koningsberger and R. Prins, *X-ray Absorption Techniques of EXAFS, SEXAFS and XANES* (Wiley, New York, 1988).
[19] E. A. Stern *et al.*, Physica (Amsterdam) **208B&209B**, 117 (1995); http://FEFF.phys.washington.edu/.
[20] F. Bridges *et al.*, Phys. Rev. B **61**, R9237 (2000).
[21] M. Croft *et al.*, Phys. Rev. B **55**, 8726 (1997).
[22] G. Subías *et al.*, Phys. Rev. B **56**, 8183 (1997).
[23] J. García *et al.*, J. Phys. Condens. Matter **13**, 3229 (2001).
[24] A. Abragam and B. Bleaney, *Electron Paramagnetic Resonance of Transition Ions* (Clarendon, Oxford, 1970), p. 792.
[25] R. B. Potts, Proc. Cambridge Philos. Soc. **48**, 106 (1952).
[26] J.-S. Wang, R. H. Swendensen, and R. Kotecký, Phys. Rev. B **42**, 2465 (1990).